Optimization of Temperature Distributions for Regional Hyperthermia Based on a Nonlinear Heat Transfer Model

Bodo Erdmann, Jens Lang, Martin Seebass

Konrad–Zuse–Zentrum für Informationstechnik Berlin
Takusstr. 7, 14195 Berlin, Germany.
e–mail: {erdmann,lang,seebass}@zib.de

Abstract. We describe an optimization process specially designed for regional hyperthermia of deap seated tumors in order to achieve desired steady–state temperature distributions. A nonlinear three–dimensional heat–transfer model based on temperature–dependent blood perfusion is applied to predict the temperature. Optimal heating is obtained by minimizing an integral object function which measures the distance between desired and model predicted temperatures. Sequential minima are calculated from successively improved constant–rate perfusion models employing a damped Newton method in an inner iteration. Numerical results for a Sigma 60 applicator are presented.

1 Introduction

Hyperthermia, i.e., heating tissue to 42 - 43$^\circ C$, is a method of cancer therapy. It is normally applied as an additive therapy to enhance the effect of conventional radio- or chemotherapy. The standard way to produce local heating in the human body is the use of electromagnetic waves. We are mainly interested in regional hyperthermia of deap seated tumors. For this type of treatment usually a phased array of antennas surrounding the patient is used (see Fig. 1). The distribution of absorbed power within the patient's body can be steered by selecting the amplitudes and phases of the antennas' driving voltages. The space between the body and the antennas is filled by a so-called water bolus to avoid excessive heating of the skin.
From the viewpoint of computational medicine there are different challenges: 1. modelling and calculation of the electromagnetic field and the forced temperature, 2. optimization of the channel adjustments to achieve favourable interference patterns for a successfull cancer therapy, 3. visualization of vector fields and temperature distributions on a very complicated geometry. All components have to be done for each individual patient within a medical planning system [1].
The purpose of our paper is to describe an optimization process based on a three–dimensional nonlinear heat transfer model. It is a rather difficult task to establish an appropriate physical model for the heat transport in the human body. Several

approaches can be found in the literature (see eg. [14, 6]). The basis for our modelling is Pennes' bio–heat–transfer equation which we equip with a temperature–dependent blood perfusion. A similar two–dimensional model was studied in [13] for ferromagnetic thermoseed hyperthermia.
To start the optimization process a specially designed object function is defined. Our aim is to get a temperature distribution which nearly avoids "hot spots" in healthy tissue and "cold spots" in the tumor region. In order to derive a fast optimization we approximate the nonlinear model by a sequence of linear ones which can be optimized very fast by applying a superposition principle.
Adaptive finite elements methods in space and linearly implicit integrators in time with step size control are used to solve the nonlinear bio–heat–transfer equation [7]. The implementation requires modern software design and programming languages as C or C++. Our code KARDOS is based on the programming environment KASKADE [3]. Additionally, a comfortable visualization tool is invaluable. We used the graphical system HYPERPLAN [1] for the presentation of our numerical results.

2 Nonlinear Heat Transfer Model

The basis model used in our simulation is the instationary bio–heat–transfer equation proposed by Pennes [10]

$$\rho c \frac{\partial T}{\partial t} = \operatorname{div}(\kappa \operatorname{grad} T) - c_b W (T - T_b) + Q_e \ , \tag{1}$$

where ρ is the density of tissue, c and c_b are specific heat of tissue and blood, κ is the thermal conductivity of tissue; T_b is the blood temperature; W is the mass flow rate of blood per unit volume of tissue. The power Q_e deposited by an electric field E in a tissue with electric conductivity σ is given by

$$Q_e = \frac{1}{2}\sigma |E|^2 \ . \tag{2}$$

The total electric field E can be computed by superposition of fields generated by different channels E_j, $j = 1, \ldots, N_{chan}$,

$$E = \sum_{j=1}^{N_{chan}} a_j \ exp(-i\theta_j) \ E_j, \tag{3}$$

where the channel j has amplitude a_j and phase delay θ_j. If complex values z_j are defined as

$$z_j = a_j \ exp(-i\theta_j) \tag{4}$$

the absorbed power Q_e can be expressed as a quadratic function of z_j

$$Q_e = \frac{1}{2}\sigma \sum_{j,k=1}^{N_{chan}} z_j^* E_j^* E_k z_k \ . \tag{5}$$

Besides the differential equation boundary conditions determine the temperature distribution. The heat exchange between body and water bolus can be described by the flux condition

$$\kappa \frac{\partial T}{\partial n} = \beta (T_{bol} - T) \tag{6}$$

where T_{bol} is the bolus temperature and β is the heat transfer coefficient. No heat loss is assumed in remaining regions. We use for our simulations $\beta = 45 W/m^2/^o C$ and $T_{bol} = 25^o C$.

Studies that predict temperatures in tissue models usually assume a constant–rate blood perfusion within each tissue. However, several experiments have shown that the response of vasculature in tissues to heat stress is strongly temperature–dependent [12]. When heated up to $41-43^o C$, temperatures that are commonly used in clinical hyperthermia, the blood flow in normal tissues, e.g., skin and muscle, increases significantly. In contrast, the tumor zone often appears to be so vulnerable to heat that the blood flow decreases upon heating.

We assume a temperature dependence of blood perfusion similar to [13]. For tumor tissue our curve has the same shape as the curve for tumor core used in [13], only the minimal and maximal perfusion differ. For muscle tissue we use a simplified curve consisting of a Gaussian profile describing the perfusion increase between $37^\circ C$ and $45^\circ C$, and a plateau for temperatures above $45^\circ C$. In the raising part our curve differs only slightly from the one used in [13], the differences are small compared to the uncertainties of the underlying experimental data [12]. For temperatures above $45^\circ C$, in [13] a decrease of perfusion is assumed. This is motivated by the assumption that vasculature is destroyed if tissue is heated to such temperatures for about 30 minutes. Our optimization process guarantees that in the steady state the temperature in healthy tissue is always below this barrier. For fat tissue we also assume a temperature dependence of blood perfusion. We apply a curve with the same shape as for muscle tissue.

Temperature–dependent blood perfusion in muscle:

$$W_{muscle} = \begin{cases} 0.45 + 3.55 \exp\left(-\dfrac{(T-45.0)^2}{12.0}\right), & T \le 45.0 \\ 4.00\,, & T > 45.0 \end{cases} \tag{7}$$

Temperature–dependent blood perfusion in fat:

$$W_{fat} = \begin{cases} 0.36 + 0.36 \exp\left(-\dfrac{(T-45.0)^2}{12.0}\right), & T \le 45.0 \\ 0.72\,, & T > 45.0 \end{cases} \tag{8}$$

Temperature–dependent blood perfusion in tumor:

$$W_{tumor} = \begin{cases} 0.833\,, & T < 37.0 \\ 0.833 - (T - 37.0)^{4.8}/5.438E{+}3\,, & 37.0 \le T \le 42.0 \\ 0.416\,, & T > 42.0 \end{cases} \tag{9}$$

The material properties of the involved tissues are summarized in Tab. 1. For blood we take $T_b = 37^oC$, $c_b = 3500Ws/kg/^oC$, and $\rho_b = 1000kg/m^3$. If a constant–rate perfusion model is applied, we set $W = 0.54kg/s/m^3$ for fat, $W = 0.833kg/s/m^3$ for tumor, and $W = 2.3kg/s/m^3$ for muscle.

Tissue	Thermal conductivity κ $[W/m/^\circ C]$	Electric conductivity σ $[1/m/\Omega]$	Density ρ $[kg/m^3]$	Specific heat c $[Ws/kg/^\circ C]$	Mass flow rate W $[kg/s/m^3]$
Fat	0.210	0.04	900	3,500	W_{fat} (8)
Tumor	0.642	0.80	1,000	3,500	W_{tumor} (9)
Bladder	0.600	0.60	1,000	3,500	5.000e-6
Kidney	0.577	1.00	1,000	3,500	66.670e-6
Liver	0.640	0.60	1,000	3,500	16.670e-6
Muscle	0.642	0.80	1,000	3,500	W_{muscle} (7)
Bone	0.436	0.02	1,600	1,000	0.450e-6
Aorta	0.506	0.86	1,000	3,500	83.330e-6
Intestine	0.550	0.60	1.000	3,500	3.333e-6

Table 1: Material properties of tissues.

The stationary temperature field T can be computed as sum of the basal temperature T_{bas} determined by $Q_e = 0$, and the incremental temperature T_{inc} due to the hyperthermic application. We easily derive the stationary equations for T_{bas} and T_{inc}

$$\begin{aligned} \operatorname{div}(\kappa \operatorname{grad} T_{bas}) - c_b W[T_{bas}](T_{bas} - T_b) &= 0\,, \\ \kappa \frac{\partial T_{bas}}{\partial n} - \beta(T_{out} - T) &= 0\,, \end{aligned} \tag{10}$$

and

$$\begin{aligned} \operatorname{div}(\kappa \operatorname{grad} T_{inc}) - c_b(\, W[T_{inc} + T_{bas}]T_{inc} & \\ +(\, W[T_{inc} + T_{bas}] - W[T_{bas}]\,)\,(T_{bas} - T_b)\,) + Q_e &= 0\,, \\ \kappa \frac{\partial T_{inc}}{\partial n} + \beta T_{inc} &= 0\,. \end{aligned} \tag{11}$$

This splitting allows us to clearly distinguish between local effects forced by the permanent cooling of the human body at the surface and the heating by the electromagnetic field. Therefore, in an adaptive approach most of the refinement can be concentrated in regions where the power Q_e is large, e.g., in the tumor zone.

3 Grid Generation and Adaptive FEM

For patient specific treatment planning we create a tetrahedral model based on a set of CT-scans of the patient. Prior to grid generation, a segmentation of the CT data is performed, i.e., the relevant tissue compartments are defined on each scan.

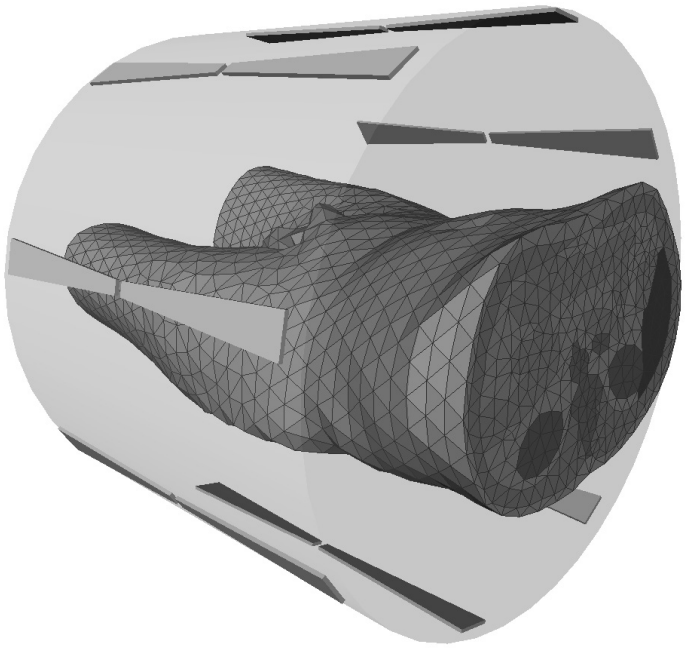

Fig. 1: Patient model (torso) and hyperthermia applicator. The patient is surrounded by 8 antennas emitting radiowaves. A water–filled bolus is placed between patient and antennas.

Our method for generating a patient model consists of three steps:
First we extract the compartment surfaces from the segmented CT data. For this purpose we have generalized the marching cubes algorithm [8], which is well-known in computer graphics, for non-binary classifications [5]. Our method creates a consistent description of the compartment interfaces. They are composed of so-called patches each separating two different compartments.
Second we perform a coarsening of the patches to get surfaces suitable for tetrahedron generation. We estimate the principal curvatures of the patches to be remeshed, and adapt the triangle size to surface curvature. For remeshing we use an advancing front method: Starting from the boundary of a patch we cover the whole patch with triangles.
Third we fill each tissue compartment with tetrahedra. Again we use an advancing front method. The compartment's surface is composed from the correspond-

ing patches. At the beginning the advancing front is identical with this surface. Then repeatedly a triangle of the advancing front is selected and a fourth point is searched such that the resulting tetrahedron resembles an equilateral one as much as possible. This procedure is continued until the whole compartment is filled with tetrahedra [11].
The derived tetrahedral patient model is the basis for the formulation of a finite element method to approximate the bio–heat–transfer equation. We solve it adaptively both in time and space [7] in order to get efficiently more accurate solutions. In [4] simulations with coarse and adaptively improved grids indicated significant differences in the tissue temperatures. We discretize time first and approximate the momentary temperature by continuous piecewise linear functions. Refinement takes place in those regions where the estimated error is higher than a prescribed tolerance. A multilevel iterative solution of the arising linear systems provides optimal computational complexity.

4 Optimization Process

Our goal is to control the amplitudes z_j, $j = 1, \ldots, N_{chan}$, of the independent channels in order to achieve an effective hyperthermia therapy. A favourable temperature distribution is characterized as follows:

1. Within the tumor a therapeutic temperature level of $42 - 43^oC$ is reached.
2. No larger regions of healthy tissue are heated to above $42 - 43^oC$.
3. Temperature in healthy tissue does not exceed certain temperature limits depending on the tissue type.

Taking into account these requirements we define an object function for optimizing the temperature field

$$q = \int\limits_{\substack{x \in \text{ tumor} \\ T < T_{ther}}} (T_{ther} - T)^2 \, dx \; + \int\limits_{\substack{x \notin \text{ tumor} \\ T > T_{health}}} (T - T_{health})^2 \, dx \; + \; p \int\limits_{\substack{x \notin \text{ tumor} \\ T > T_{lim}}} (T - T_{lim})^2 \, dx \; , \quad (12)$$

where we use a therapeutic level $T_{ther} = 43^oC$, and a temperature $T_{health} = 42^oC$ that should not be exceeded in healthy tissue. The limits T_{lim} are chosen tissue–dependent: $T_{lim} = 42^oC$ for more sensible tissue compartments (bladder, intestine) and $T_{lim} = 44^oC$ otherwise. To ensure high penalization for temperatures exceeding the limits we set $p = 1000$.
The definition of the object function as an integral of squares guarantees that regions with large deviations from the attempted temperatures, i.e., "hot spots" in healthy tissue and "cold spots" in the tumor, contribute large amounts to the object function. A similar optimization strategy for a phased array hyperthermia system based on a simpler object function is described in [9].
Optimization of the temperature distribution means to choose the amplitudes z_j

of each channel in such a way that the resulting temperature field minimizes the object function q.
Using our piecewise linear finite element solution T_h and applying an integration formula based only on the vertices x_i (mass lumping), we get an approximation of the object function

$$q_h = \sum_{i \in M_{h1}} \frac{w_i}{4}(T_{ther} - T_h(x_i))^2 + \sum_{i \in M_{h2}} \frac{w_i}{4}(T_h(x_i) - T_{health})^2 + p \sum_{i \in M_{h3}} \frac{w_i}{4}(T_h(x_i) - T_{lim})^2 \tag{13}$$

with

$$\begin{aligned} M_{h1} &= \{\text{i: } x_i \in \text{tumor}, T_h(x_i) < T_{ther}\}, \\ M_{h2} &= \{\text{i: } x_i \notin \text{tumor}, T_h(x_i) > T_{health}\}, \\ M_{h3} &= \{\text{i: } x_i \notin \text{tumor}, T_h(x_i) > T_{lim}\}, \end{aligned}$$

where w_i stands for the volume of all tetrahedra of which x_i is a vertex.
In a next step we derive formulas which allow us to compute quickly a new temperature field for changing amplitudes. Let us first consider the linear model with a constant–rate perfusion in each tissue. Then from (11) it can be directly seen that T_{inc} depends linearly on the distribution of absorbed power Q_e. Hence, a superposition principle is valid:

$$T_{inc}(\alpha_1 Q_e^1 + \alpha_2 Q_e^2) = \alpha_1 T_{inc}(Q_e^1) + \alpha_2 T_{inc}(Q_e^2)\,. \tag{14}$$

According to the representation (5) we get

$$T_{inc}(Q_e) = \sum_{j,k=1}^{N_{chan}} z_j^*\, T_{inc}(E_j^* E_k)\, z_k\ , \tag{15}$$

and finally for the whole stationary temperature distribution

$$T(Z) = T_{bas} + \sum_{j,k=1}^{N_{chan}} z_j^*\, T_{inc}(E_j^* E_k)\, z_k\ , \tag{16}$$

where Z is the vector of all z_j. The incremental temperatures $T_{inc}(E_j^* E_k)$ can be derived from N_{chan}^2 basic calculations combining two channels. Consequently, for an arbitrary set of parameters z_j the object function can be computed very fast. This is also true for the first and second derivatives of the finite element solution T_h with respect to the parameters z_j.
In the nonlinear case, relation (14) is no longer valid. Nevertheless, we can fix the nonlinear perfusion terms due to a given intermediate state Z_n of all amplitudes. Then we utilize representation (15) as an approximation in a neighborhood of Z_n to perform the minimization process. Doing so we get a better Z_{n+1} for which we solve the nonlinear heat equation. The arising perfusion $W(T(Z_{n+1}))$ is once

again fixed and the optimization is done. Improving successively the constant–rate model of the perfusion in such a way, we end up with a nearly optimal adjustment of the parameters z_j for the nonlinear model.
Employing a damped Newton method for the optimization, the iteration can be described as follows:

Choose initial value $Z_0^{(0)}$

for $n = 0, 1, \ldots$

Calculate stationary temperature $T(Z_n^{(0)})$

Calculate $W_n := W(T(Z_n^{(0)}))$

Calculate $T_{\text{inc}}(E_j^* E_k)$, $j, k = 1, \ldots, N_{\text{chan}}$, employing W_n

for $k = 0, 1, \ldots$

Calculate $D^i q_h := \left. \frac{D^i q_h}{dZ^i} \right|_{Z=Z_n^{(k)}}$, $i = 1, 2$

Calculate $\Delta Z := -(D^2 q_h)^{-1} D^1 q_h$

Find $\alpha_0 \in \{1, \frac{1}{2}, \frac{1}{4}, \ldots\}$ **such that**

$q_h(Z_n^{(k)} + \alpha_0 \Delta Z) < q_h(Z_n^{(k)}) + \frac{1}{2}\alpha_0 D^1 q_h \Delta Z$

Define $Z_n^{(k+1)} := Z_n^{(k)} + \alpha_0 \Delta Z$

Finished?

Define $Z_{n+1}^{(0)} := Z_n^{(k+1)}$

Finished?

The inner iteration is terminated if the object function has changed by less than 0.02 within 10 iterations. To control the outer iteration we always compute the new stationary temperature $T(Z_{n+1}^{(0)})$ and compare it with the old one. If the difference becomes small enough (less than $0.05^{\circ}C$), we stop the optimization process.

5 Numerical Results

We report some data concerning a concrete optimization process for an individual patient. The used applicator consists of eight radio frequency antennas grouped in four antenna pairs (Sigma 60 Applicator of the BSD 2000 Hyperthermia System). Each group can have its own amplitude and phase. So, our aim is to control four

different complex values z_j.

n	0	1	2	3	4	5
q_h	1732	1458	1327	1263	1229	1214
$\|\delta T\|_\infty$	-	3.5	0.7	0.18	0.085	0.043

Tab. 2: Data of optimization process.

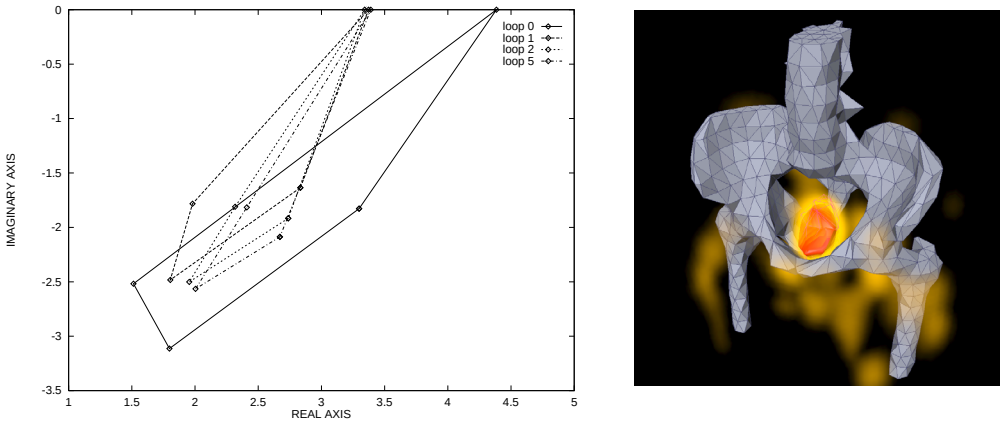

Fig. 2: Optimization of the four complex amplitudes plotted in a quadrilateral for each outer iteration step (left); optimized temperature distribution (right).

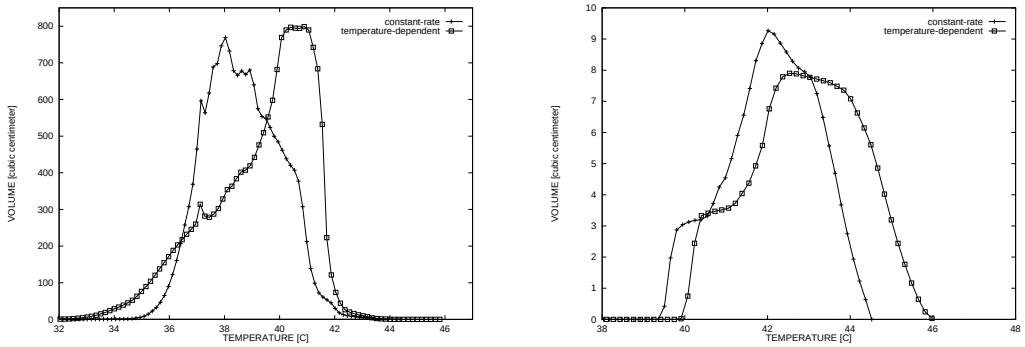

Fig. 3: Temperature–volume histograms for muscle (left) and tumor tissue (right) showing the differences between constant–rate and temperature–dependent perfusion.

First, we calculate an initial optimized $Z_0^{(0)}$ employing our constant–rate perfusion model. Then we proceed as described in Section 4. The optimization comes to an end after five outer iteration steps. The corresponding values of the object function q_h and the maximal temperature difference are shown in Tab. 2.
In Fig. 2 the convergence history of the vector $Z_n^{(0)}$ is presented. For each outer

iteration step all complex amplitudes z_j are plotted as vertices of a quadrilateral. We observe that the use of the nonlinear heat transfer model leads to a more uniform adjustment of $|z_j|$ and to a slight reduction of the phase differences.
The smaller value of the object function for the nonlinear model (see Tab. 2) results from a better tumor heating (Fig. 2, right), which is also reflected by the temperature–volume histogram for tumor tissue shown in Fig. 3. The histogram for muscle tissue reveals that assuming the nonlinear model a much larger amount of tissue is heated above 40^oC.

Acknowledgement. The authors are indebted to P. Deuflhard for his continuing support of this project. This work was partially supported by Deutsche Forschungsgemeinschaft, SFB 273.

References

[1] Beck, R., Deuflhard, P., Hege, H.-C., Seebass, M., Stalling, D., Numerical Algorithms and Visualization in Medical Treatment Planning, Preprint SC 96–54, Konrad–Zuse–Zentrum für Informationstechnik Berlin, Germany

[2] Bornemann, F., Erdmann, B., Kornhuber, R., 1993, Adaptive multilevel methods in three space dimensions, *Int. J. Num. Meth. Engrg.* **36**, 3187–3203

[3] Erdmann, B., Lang, J., Roitzsch, R., 1993, *KASKADE – Manual*, Technical Report TR 93–05, Konrad–Zuse–Zentrum für Informationstechnik Berlin, Germany

[4] Erdmann, B., Lang, J., Seebass, M., 1997, Adaptive Solutions of Nonlinear Parabolic Equations with Application to Hyperthermia Treatments, *Proc. Int. Symp. on Advances in Comp. Heat Transfer, Cesme*

[5] Hege, H.-C., Seebass, M., Stalling, D., Zöckler, M., 1997, A Generalized Marching Cubes Algorithm Based On Non-Binary Classifications, Preprint SC 97–05, Konrad–Zuse–Zentrum für Informationstechnik Berlin, Germany

[6] Kotte, A., van Leeuwen, J., de Bree, J., van der Koijk, J., Crezee, H., Lagendijk, J., 1996, A description of discrete vessel segments in thermal modelling of tissues, *Phys. Med. Biol.* **41**, 865–884

[7] Lang, J., 1997, Adaptive FEM for Reaction–Diffusion Equations, to appear in *Appl. Numer. Math.*

[8] Lorensen, W.E., Cline, H.E., 1987, Marching Cubes: A high resolution 3D surface construction algorithm, *Computer Graphics* **21**, 163-169

[9] Nikita, K.S., Maratos, N.G., Uzunoglu, N.K., 1993, Optimal Steady–State Temperature Distribution for a Phased Array Hyperthermia System, *IEEE Trans. Biomed. Engrg.* **40**, 1299–1306

[10] Pennes, H.H., 1948, Analysis of tissue and arterial blood temperatures in the resting human forearm, *J. Appl. Phys.* **1**, 93–122

[11] Seebass, M., Stalling, D., Nadobny, J., Wust, P., Felix, R., Deuflhard, P., 1996, Three-Dimensional Finite Element Mesh Generation for Numerical Simulations of Hyperthermia Treatments, in C. Franconi, G. Arcangeli, and R. Cavaliere (eds.), *Proc. 7th Int. Congress on Hyperthermic Oncology, Roma* Vol. 2, 547-548

[12] Song, C. W., Lokshina, A., Rhee, J. G., Patten, M., Levitt, S. H., 1984, Implication of Blood Flow in Hyperthermic Treatment of Tumors, *IEEE Trans. Biomed. Engrg.* **31**, 9–16

[13] Tompkins, D. T., Vanderby, R., Klein, S.A., Beckman, W.A., Steeves, R.A., Frey, D.M., Palival, B.R., 1994, Temperature–dependent versus constant–rate blood perfusion modelling in ferromagnetic thermoseed hyperthermia: results with a model of the human prostate, *Int. J. Hyperthermia, Vol.* **10**, No. 4, 517–536

[14] Weinbaum, S., Jiji, L.M., 1985, A new simplified bioheat equation for the effect of blood flow on local average tissue temperature, *J. Biomech. Eng. Trans. ASME* **107**, 131–139